NIFS concentric integral field unit*

John Hart[a], Peter McGregor[a], and Gabe Bloxham[a]

[a]Research School of Astronomy and Astrophysics, Australian National University, Cotter Rd., Weston, ACT 2611, Australia

ABSTRACT

The Gemini Near-infrared Integral Field Spectrograph (NIFS) will be used with the ALTAIR adaptive optics system on Gemini North. NIFS uses a reflective, concentric, integral field unit (IFU) to reformat its focal plane. The concentric IFU design integrates the IFU with the spectrograph collimator to form a dedicated IFU instrument. The IFU channels are identical and fanned about a single axis passing through the image slicer. The spherical optical surfaces of the spectrograph collimator are all concentric and centered on this fanning axis. The grating is also located on the fanning axis, and the system is arranged to produce coincident pupil images at the grating. In this way, each channel of the IFU performs as if it is on-axis. This avoids complications due to off-axis angles that are intrinsic to other reflective IFU designs.

Keywords: near-infrared, spectrograph, integral field unit

1. INTRODUCTION

The Gemini Near-infrared Integral Field Spectrograph (NIFS)[1,b] will be used for near diffraction-limited imaging spectroscopy with the ALTAIR facility adaptive optics system on Gemini North. The integral field unit (IFU) at the heart of NIFS is an evolution and a simplification of the reflective IFU design proposed by Content[2]. Reflective IFUs, compared to other IFU types, offer advantages of high throughput and high packing efficiency on the detector. Diamond machined metal optics for near-infrared applications offer further advantages of good mechanical stability at cryogenic temperatures and versatility of surface forms. Fanning of the IFU channels in conventional reflective IFU designs leads to increasing off-axis angles that become more severe as IFU field size increases. NIFS uses a novel IFU design that avoids this dilemma by fanning each IFU channel about the image slicer axis, and making each IFU channel, as well as the spectrograph collimator and grating pupil, rotationally symmetric about this axis. The spectrograph collimator then becomes an integral part of the IFU instrument, and the optical performance of the IFU is greatly improved.

2. IFU CONCEPTS

IFUs have been developed in three basic forms; pupil imaging systems such as TIGER[3] and SAURON[4], fiber IFUs such as SPIRAL[5] and the GMOS[6] IFU, and reflective IFUs such as originally implemented in 3D[7]. The 3D reflective IFU (Figure 1 *left*) used a stack of thin plane mirrors at an image plane as an *image slicer* that fanned out the IFU channels, then an array of plane beam-steering mirrors each placed on a hyperbolic locus to direct beams from each IFU channel to a single grating pupil. This arrangement worked well for the 16×16 spatial elements possible with early 256×256 pixel near-infrared detectors. However, extension of this approach to larger fields-of-view and larger detector formats leads to complications in that the beams from adjacent IFU channels overfill their beam-steering mirrors, which in turn leads to unacceptable cross-talk. Adjacent beam steering mirrors can be offset in a brickwork pattern by tilting the corresponding image slicer mirrors[8], but a trade-off still has to be made between slow enough beams to make the image slicer mirrors manufacturable and fast enough beams to reduce the physical length of the reformatted slit so that the

[b] http://www.mso.anu.edu.au/nifs

collimator optics are manageable. The solution proposed by Content[2] is to apply power to the image slicer mirrors so that pupil images are formed on the beam-steering mirrors (Figure 1 *right*). In this way, the divergence of the IFU beams is controlled and cross-talk is eliminated. These beam-steering mirrors in the pupil plane are referred to as *pupil mirrors*. In practice, the input field is reimaged onto the image slicer at an enlarged scale using fore-optics in ordered to increase the slicer mirror thickness and hence ease their manufacture. Slowing the beam onto the image slicer also reduces the fanning angles required, which in turn reduces cross-talk due to image defocus at extreme image slicer mirror displacements. The pupil mirrors in this design also have power in order to reimage the field of each IFU channel at a scale and focal ratio appropriate for the spectrograph collimator. The reformatted slit length is then defined by the faster focal ratio of the collimator, rather than by the slower focal ratio of the image slicer. The severe beam divergence that would otherwise result from the proximity of the pupil images to the reformatted focal plane is avoided by the addition of *field mirrors* at the reformatted "staircase" slit image plane. These field mirrors direct the individual IFU beams to a single pupil at the grating.

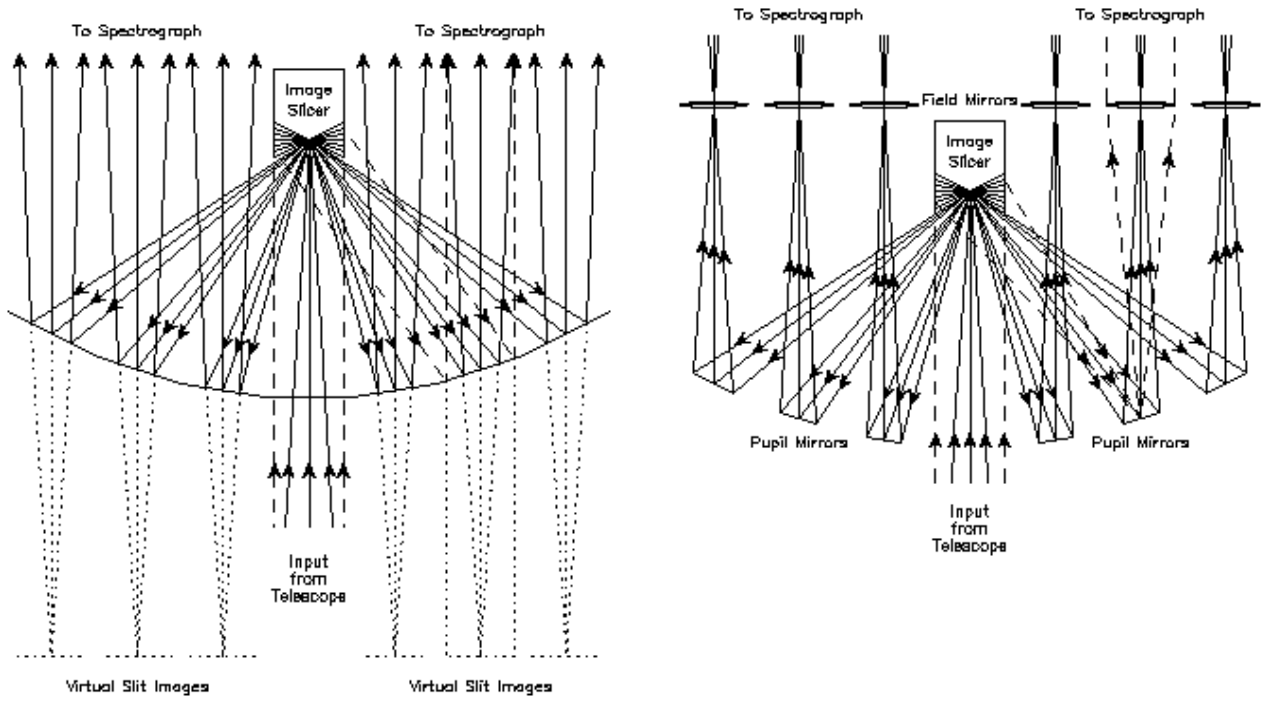

Figure 1: Schematic optical layout of the 3D IFU (*left*) and the Content[2] IFU (*right*).

The Content[2] IFU design is intended to feed an existing spectrograph that is also used for conventional long slit spectroscopy. As such, the IFU is required to produce an essentially telecentric output that appears to the spectrograph collimator to have originated from the telescope itself. The requirement to derive a telecentric output from a fanned (non-telecentric) input demands that the IFU deals with channels that become progressive more off-axis towards the edges of the IFU field. These increasing off-axis angles have four effects; 1) they produce aberrations in the image, 2) the pupil images produced by the image slicer are progressively more defocused relative to the vertex plane of the central pupil, 3) the pupil images are formed low on the pupil mirrors of extreme IFU channels (consider the intersection of a shallow angle cone with a tangent plane) and hence different IFU channels form pupils at different locations on the grating, and 4) the individual pupil mirrors of off-axis IFU channels must be progressively decentered to steer the fanned beams back parallel to the optical axis. The latter effect precludes the use of a monolithic diamond machined pupil mirror array (see §4.2). Any easily manufactured solution that we identified that did not individually customize the surfaces of every pupil mirror produced compromised optical performance due to aberrations introduced by the off-axis angles.

The solution has been to adopt the concentric IFU design that treats each IFU channel identically, as if it is on the optical axis. However, in doing so it has been necessary to abandon the telecentric output and integrate the IFU with the spectrograph collimator to form a dedicated NIFS IFU instrument. The NIFS optical layout is shown in Figure 2. A spherical concave tilted *f-converter* mirror first reimages the f/16 ALTAIR focal plane at f/256 onto the imager slicer, and in doing so forms a 4.0 mm diameter pupil image at a reflective cold stop. The 2.99"×2.99" image of the sky formed on the image slicer is divided into 29 strips each 0.103" wide by the 1.024 mm thick image slicer mirrors (Figure 3 *right*). The image slicer mirrors are rotated about a vertical axis passing through the front face of the central mirror, i.e., the *fanning axis*. Each image slicer mirror is spherically concave so that it produces a pupil image on the corresponding element of the pupil mirror array. Before fanning, the image slicer mirrors are each part of a common concave spherical surface having a radius of curvature of ~ 623 mm. The pupil images are arranged to under-fill the elements of the pupil mirror array with a comfortable margin. The 29 pupil mirrors lie on a continuous concave arc that is also centered on the fanning axis (Figure 3 *left*). Each pupil mirror is torically concaved by an amount needed to produce a good image of its image slicer mirror on the corresponding element of the field mirror array. The 29 field mirrors lie on a corresponding continuous convex arc that is again centered on the fanning axis. The focal ratio at the field mirror array is f/16. The images of adjacent image slicer mirrors on the field mirror array are stacked in staircase form (i.e., corner-to-corner) along the field mirror array. Each element of the field mirror array is torically concaved to produce good pupil images at the grating. The pupil and field mirror arrays are separated by 27.888 mm, and are both tilted by 5º with respect to the central ray to allow for entry and exit beam clearance. The field mirrors feed the Bouwers collimator of the spectrograph, which consists of a spherical primary mirror and a concentric spherical meniscus that corrects the spherical aberration of the primary. The three Bouwers collimator surfaces (primary and two corrector surfaces) are concentric with the fanning axis. The field mirror array must be positioned equidistant from the imager slicer and the collimator primary so that each IFU channel forms an image of its pupil on the fanning axis below the image slicer, where the grating is located. The use of concentric optical surfaces through the IFU to the grating pupil eliminates off-axis angles in the IFU, but requires a length of ~ 840 mm to accommodate the Bouwers collimator.

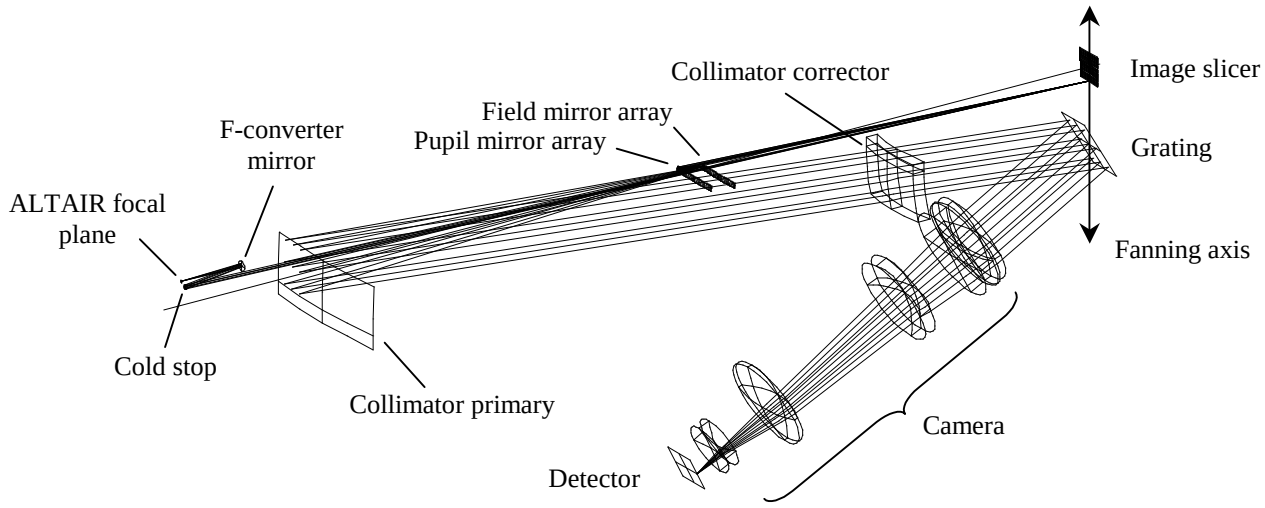

Figure 2: NIFS optical layout showing the concentric IFU at top with fold mirrors omitted. Rays are shown for the far channel of the IFU. Optical components are labeled.

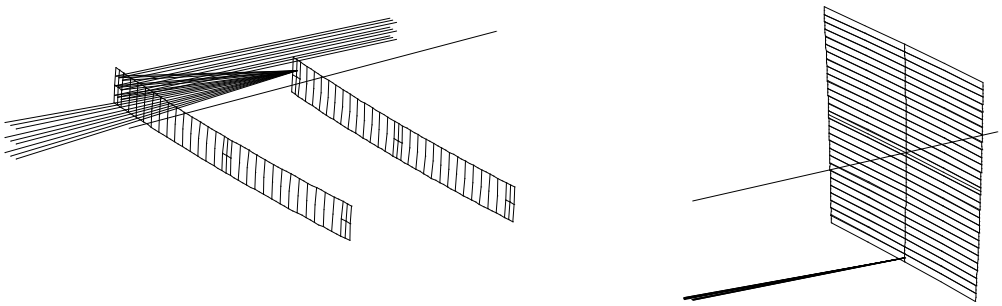

Figure 3: Image slicer (*right*) showing 29 slitlet mirrors each fanned by 0.127º, and pupil and field mirror arrays (*left*) showing rays for the far IFU channel. The orientation is the same as in Figure 1.

NIFS operates near the diffraction-limit. The 0.1" wide NIFS image slicer mirrors are comparable in width to the telescope diffraction size (~ 0.06" FWHM at *K*). Diffraction at the imager slicer mirrors broadens the pupil images at the pupil mirrors in the dispersion direction, which is perpendicular to the pupil mirror array. The pupil mirrors and the spectrograph gratings are made larger by ~ 60% than their geometrical pupil sizes in this direction to capture as much as is practical of this diffracted light. Even so, truncation of the grating pupil image by the grating is expected to result in some unavoidable ringing in the spectrograph resolution profile[1].

3. CONCENTRIC IFU DESIGN

3.1 F-converter magnification

The IFU geometry must be arranged so that the width of the pupil images on the pupil mirror array is comfortably less than the width of the mirror elements. For a concentric IFU, the pupil fill factor is given by

$$k = \frac{f_{col} d_{tel}}{M_c M f_{tel}^2 \theta_y} \tag{1}$$

where f_{col} is the collimator focal length, d_{tel} is the telescope aperture diameter, M_c is the input f-converter magnification, $M = M_c M_p$ is the combined input f-converter and pupil mirror magnification, f_{tel} is the telescope focal length, and θ_y is the angular size of the IFU field in the spatial direction. Except for the input f-converter magnification, all of the independent parameters in Equation (1) are determined by other design requirements. The pupil fill factor must not be greater than 1, so this places a lower limit on the f-converter magnification:

$$M_c \geq \frac{f_{col} d_{tel}}{M f_{tel}^2 \theta_y} . \tag{2}$$

For $M = 1$, $f_{col} = 418.32$ mm, $d_{tel} = 7891$ mm, $f_{tel} = 128000$ mm, and $\theta_y = 14.51$ μrad (3.0"), M_c must be greater than 13.9. NIFS uses $M_c = 16$ so that the pupil images are comfortably smaller than the pupil mirror array elements ($k = 0.868$). Larger f-converter magnifications would provide more clearance, but would also increase aberrations.

3.2 IFU channel fanning geometry

The elements of the pupil mirror and field mirror arrays are located around concentric arcs centered on the fanning axis of the image slicer. The radii of these two arcs are 446.21 mm and 418.32 mm, respectively. The circumferential length of each element in the field mirror array must match the length of the image slicer mirror image projected onto it. Given that the angular length of each image slicer mirror, referred to the sky, is 14.51 μrad and the focal length at the field mirror array is 128 m, the angular fanning pitch of the IFU must be 0.2537º, the total fanning angle is 7.1036º, the circumferential pitch of the pupil mirror array elements is 1.984 mm, and the circumferential pitch of the field mirror array elements is 1.860 mm.

3.3 IFU aberrations

The pupil mirror array causes image aberrations because it must be operated off-axis. Third-order equations have been derived for these aberrations to facilitate selection of the off-axis angle. The equations apply to images at the slitlet centers and assume that the separation between the pupil and field mirror arrays is small compared to that between the image slicer and the pupil mirror array. The aberrations are referred to the sky.

The maximum angular tangential coma, $ATC_{\max}$, occurs at the most off-axis point in the field, and is given by

$$ATC_{\max} = \frac{3\theta_x K^2}{16F^2} + \frac{3K^2 c}{32 d_{tel} F^3} + \frac{3\theta_x k K^3}{64F^2} \tag{3}$$

where θ_x is the angular size of the IFU field in the spectral direction, K is the factor by which the pupil mirrors are enlarged in the spectral direction to account for diffraction at the image slicer mirrors, c is the clearance between the image slicer output beam and the image envelope on the field mirror array, and F is the focal ratio at the field mirror array.

Maximum angular astigmatism, $AAS_{\max}$, also occurs at the most off-axis point in the field, and is given by

$$AAS_{\max} = \frac{2K}{\theta_x k}\left[\frac{\theta_x}{2F} + \frac{c}{4 d_{tel} F^2} + \frac{\theta_x k K}{8F}\right]^2 . \tag{4}$$

The minimum angular astigmatism, $AAS_{\min}$, occurs at the least off-axis point in the field, and is given by

$$AAS_{\min} = \frac{2K}{\theta_x k}\left[\frac{c}{4 d_{tel} F^2} + \frac{\theta_x k K}{8F}\right]^2 . \tag{5}$$

A fixed amount of correction can be applied across the field if a toric figure is used in place of a spherical figure for the pupil mirror array elements. In fact, the maximum and minimum corrected angular astigmatism can be made to have equal magnitudes and opposite signs with the magnitude, AAS_{tor}, being half the difference between the uncorrected maximum and minimum values. AAS_{tor} is then given by

$$AAS_{tor} = \frac{AAS_{\max} - AAS_{\min}}{2} . \tag{6}$$

The angular spherical aberration (focused for minimum diameter), ASA, is given by

$$ASA = \frac{\theta_x k K^3}{128 F^2} . \tag{7}$$

Application of these equations shows that astigmatism is the dominant aberration, and that it increases rapidly as the focal ratio at the field mirror array, F, is reduced. Large values of the pupil mirror fill factor, k, and small values of clearance, c, are moderately desirable. The use of a toric rather than a spherical figure for the pupil mirror elements gives considerable image improvement. The pre-determined parameter values for the NIFS concentric IFU are d_{tel} = 8000 mm (nominal), θ_{x} = 14.5 μrad, and K = 1.6. To give good aberration control, the chosen parameter values are F = 16, k = 0.87, and c = 1.6 mm. The resulting aberrations are listed in Table 1.

Table 1: NIFS Concentric IFU Aberration Values

	$ATC_{\max}$	$ATC_{\min}$	$AAS_{\max}$	$AAS_{\min}$	AAS_{tor}	ASA
μrad	0.049	0.021	0.167	0.033	0.067	0.002
mas	10.0	4.3	34.4	6.8	13.8	0.3

3.4 IFU tilt angle

The tilt angle of the pupil and field mirror arrays is the angle required to pass the beam with adequate clearance, *c*. The required tilt angle, α, of the pupil and field mirror array elements with respect to the center ray is given by

$$\alpha = \frac{\theta_x d_{tel} F + c}{2s} + \frac{K}{4F} \tag{8}$$

where *s* is the separation between the pupil and field mirror arrays. For the adopted parameters, *s* = 28 mm so α = 5°.

3.5 IFU configuration

In the ideal concentric IFU, the channels of the IFU are fanned about a common axis that passes through the center of the image slicer in a way that makes the IFU channels optically identical. This common channel geometry should also be arranged to produce good image quality. The geometrical principles required to achieve this ideal are the following:

- The curved surface of the image slicer should be tangential to the fanning axis at its center. This is the condition for which all IFU channels have the same fixed altitude angle, and the mirror arrays are circularly symmetric. An additional desirable characteristic then follows: the azimuth angle of each image slicer mirror is exactly half of the azimuth angle of the corresponding IFU channel.

- The aluminum alloy plates onto which the pupil and field mirror elements are machined should be perpendicular to the fanning axis. This allows all the elements of the circularly symmetric mirror arrays to be mechanically centered in the plates.

- The off-axis angles for all three mirror elements in each IFU channel (image slicer, pupil mirror, and field mirror) should be made no larger than is needed to avoid beam interference with adjacent components. This minimizes astigmatism in either the field or pupil images. The image slicer and field mirrors produce aberrations only in the pupil image, so this requirement is less stringent for these elements than for the pupil mirror.

The configuration shown in Figure 4 complies with all of these principles. A characteristic of this configuration is that the pupil and field mirror elements are tilted with respect to the plates from which they are fabricated. This means that the relatively fast beam emerging from the field mirror makes a very shallow angle with respect to the pupil mirror array plate, so a clearance problem exists for the beams coming from the lower elements of the image slicer. More importantly, there are repercussions for the diamond machining of the arrays (§4); to achieve the required surface figure, the mirror array plates would have to be tilted in the diamond-machining mill and then the tool path has to be adjusted in height for each element of the array. Neither of these difficulties is intolerable, but their avoidance is very desirable. Given that the production of the IFU was seen as one of the most demanding aspects of the NIFS project, it was decided to simplify its manufacture by altering the IFU configuration.

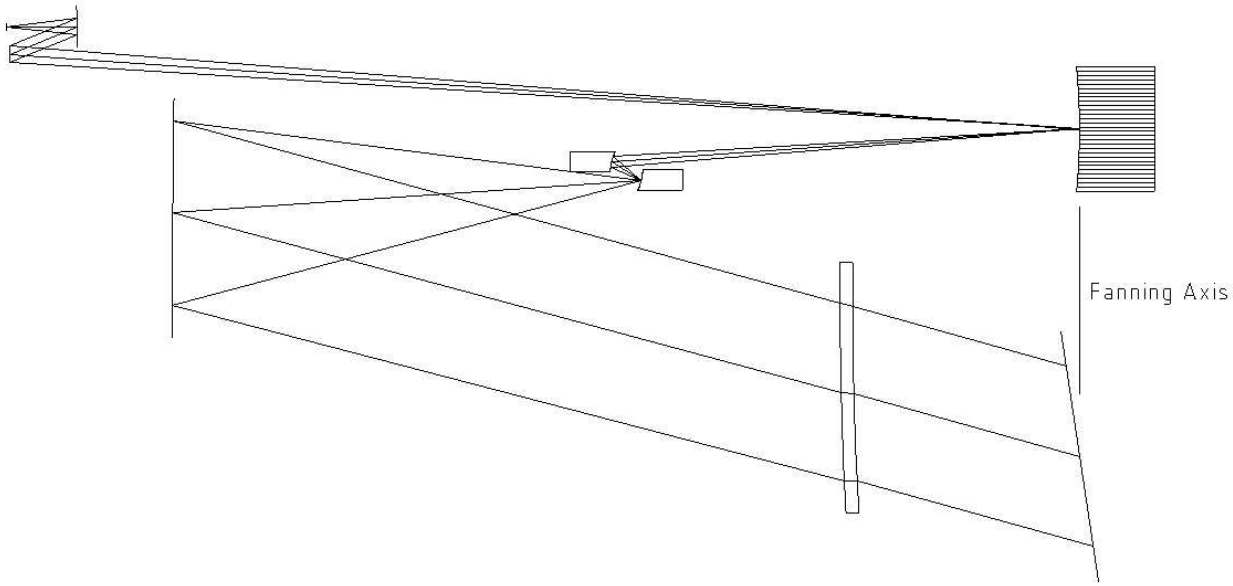

Figure 4: Ideal concentric IFU configuration shown with anamorphic distortion.

The NIFS IFU uses the configuration shown in Figure 5. This configuration violates the first of the above ideal IFU principles, in that the center of the image slicer is not tangential to the fanning axis. Rather, the curved image slicer surface (but not the mechanical stack) is tilted downward by 4º. The pupil and field mirror elements are then square to the array plates, and an appropriate off-axis angle can be chosen for the image slicer (1º in NIFS). This avoids both the clearance and the mirror array manufacturing issues of the "ideal" configuration.

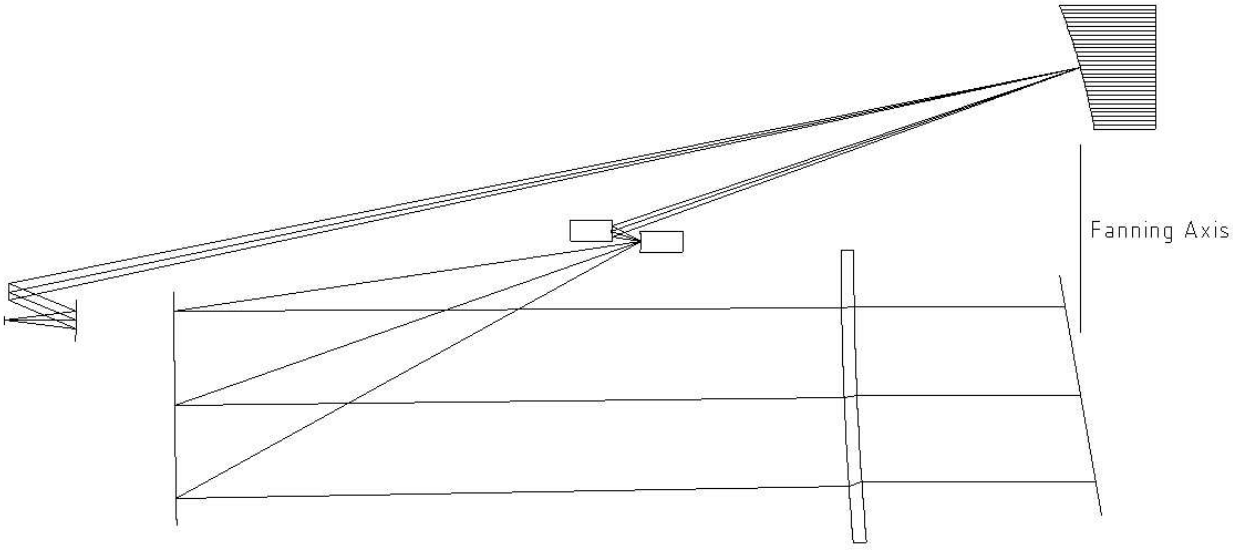

Figure 5: NIFS concentric IFU configuration shown with anamorphic distortion.

The penalty for adopting this configuration is that the fanning geometry is no longer ideal, so the altitude angle of the reflected ray varies as the azimuth angle of the image slicer mirror changes from channel to channel, and the azimuth

angle of the reflected ray is no longer simply twice the azimuth angle of the image slicer mirror. The azimuth deviation is easily corrected by adjusting the angular offsets of the image slicer mirrors, but the varying altitude angle causes the pupil images to be located at different heights on the pupil mirror array. In practice, this effect is small being < 30 μm at the pupil image, which is negligible compared to the pupil image aberration.

The analysis shown above places the axial ray in the center of the pupil mirror array element. In fact, an additional correction is made. Because the rays producing the pupil image come from an image slicer mirror that is offset from the axial ray and because there are aberrations in that image, the centroid of the pupil image is also displaced from the axial ray. To correct this, non-linear adjustments are made to the angular offsets of the image slicer mirrors, as determined by ray tracing.

4. CONCENTRIC IFU MANUFACTURE

A major challenge of the NIFS project has been the manufacture of the IFU. Diamond machining is the most suitable method of producing the optical surfaces required for all three IFU components (imager slicer, pupil mirror array, and field mirror array). The Laboratory for Precision Engineering (LFM) at the University of Bremen has already manufactured the image slicer mirrors and the pupil mirror array. Other items are scheduled.

4.1 Image slicer

The ~ 30 mm × 1.024 mm image slicer mirrors each have a spherically concaved optical surface. The geometry of the surfaces is such that, without fanning, they all form part of a single sphere. This feature facilitates manufacture. The stack of aluminum alloy plates is equipped with an accurate dual-mode registration system; one corresponding to the un-fanned configuration, and the other to the fanned configuration. The face of the stack was diamond turned to the common spherical figure while the stack was clamped in the unfanned configuration, then the stack was re-assembled in the second configuration.

The image slicer plates are registered using two pairs of precision dowel holes. The dowel pins that register the image slicer stack have a center distance of 100 mm, and their positions have been controlled to an accuracy of ~ 1 μm. The pupil image placement errors are therefore ~ ±12 μm, which is ~ 9% of the allowed margin.

The plate thickness is a crucial parameter. The spectrograph design has been adjusted to use a stock product, after its exact thickness was determined.

4.2 Mirror arrays

The pupil and field mirror array elements must be accurately aligned. The tilt error corresponding to one pixel of image shift is ~ 570 μrad for the pupil mirror array elements. Each mirror array has been machined as a monolith to achieve adequate alignment control. By machining in a single setup, the accuracy that can be achieved across a single optical element can be applied to the whole array, so relative misalignments within the array are effectively eliminated.

The depth of each array must also be accurately controlled in order to control the boundary positions between adjacent elements. This is because the curves of the optical surfaces are shallow. For the field mirror array, the depth error corresponding to a boundary displacement of one detector pixel is only 0.64 μm. Again, this is not a problem if the mirror arrays are diamond machined as a monolith in a single setup.

The pupil and field mirrors take the form of two rectangular plates with the mirror surfaces diamond machined into one of the long narrow faces. These plates can be mounted and adjusted with relative ease. For both arrays, a series of identical concaved toroidal mirror elements must be distributed along circular arcs that are centered on the common fanning axis of the IFU. The method devised to do this uses a fly-cutting technique that is illustrated in Figure 6. The Precitech Freeform 3000 at LFM uses a cutter tip spinning about the spindle axis while the blank is traversed in all three translational axes. In the plane of the array plate, the curvature radius of the generated surface is that of the fly-cutter circle. In the perpendicular projection, it is determined by the locus of the traverse.

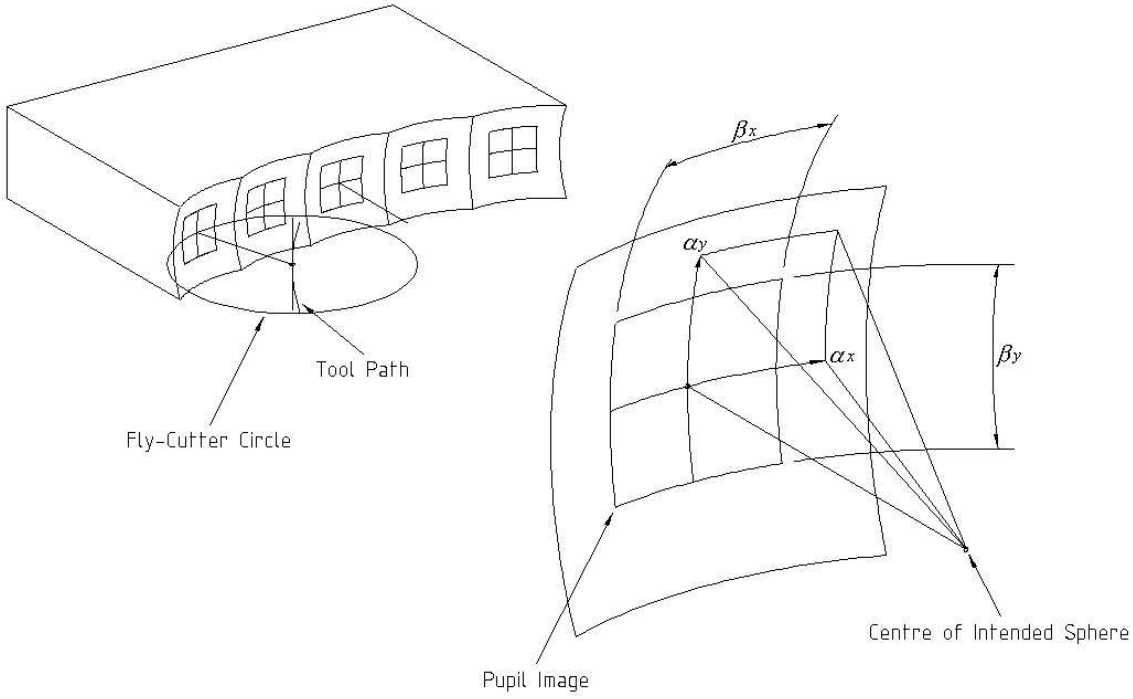

Figure 6: Fly-cutter generation geometry for pupil and field mirror arrays.

A limitation of this fly-cutting method is that it does not produce truly spherical (or toric) surfaces. Rather the surface is tangential to the intended sphere along two orthogonal lines on the surface. Elsewhere the deviation follows a "quad-foil" pattern, somewhat like the 17^{th} and 18^{th} order Zernike polynomials. A diagram of the whole fly-cutter envelope is shown in Figure 7. The shape is spherical only at the two vertices. The generation process described places one of these vertices at the center of the mirror element.

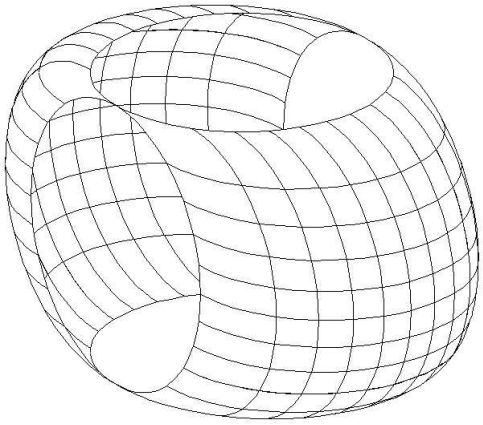

Figure 7: Wire-frame diagram of the full fly-cutter envelope. The mirror array elements utilize a small segment at one vertex of this surface.

The fly-cut pupil mirror array introduces aberrations because it is not truly toric. Figure 6 shows the geometry of the array elements. Here, the surface is only coincident with the intended toric along the α_x and α_y axes. In general, the error introduced to a ray reflected off the surface corresponds to an angular deviation on the sky of

$$\gamma_x = \frac{r\alpha_x\alpha_y^2}{2f} \text{ and } \gamma_y = \frac{r\alpha_x^2\alpha_y}{2f} \tag{9}$$

where r is the radius of curvature of the pupil mirror array elements, and f is the focal length of the telescope at the field mirror array. The angular size of the rectangular pupil (diffraction spread) on the mirror element is

$$\beta_x = \frac{1}{2F} \text{ and } \beta_y = \frac{K}{2F} \tag{10}$$

where F is the focal ratio at the field mirror array and K is the pupil enlargement factor in the spectral direction due to diffraction at the image slicer mirror. Substituting F = 16 and K = 1.6 for NIFS leads to β_x = 31.25 mrad and β_y = 50 mrad. Aberration is worst for a ray coming from the corner of the pupil image, for which $\alpha_x = \beta_x/2$ and $\alpha_y = \beta_y/2$. For r = 53 mm and f = 128000 mm, the ray deviation is γ_x = 0.002 μrad (~ 0.01 pixels) and γ_y = 0.001 μrad. These values are negligible, especially as they apply to the corner of the diffraction-spread pupil where there is very little radiation energy. Within the geometrical pupil, the fly-cutter aberration is considerably less and can be ignored.

5. MOUNTING ARRANGEMENT

5.1 Imager slicer

The imager slicer is assembled in a tower that is mounted between the two main structural elements of the spectrograph (Figure 8). The tower consists of the imager slicer stack plus top and bottom mounting blocks. The mounting blocks will be machined to align the center height of the image slicer and its tilt angle. The entire tower can be rotated on a central pin in the bottom block to permit rotation alignment. The imager slicer stack consists of two 12 mm thick aluminum anvils between which are clamped the 29 image slicer mirrors.

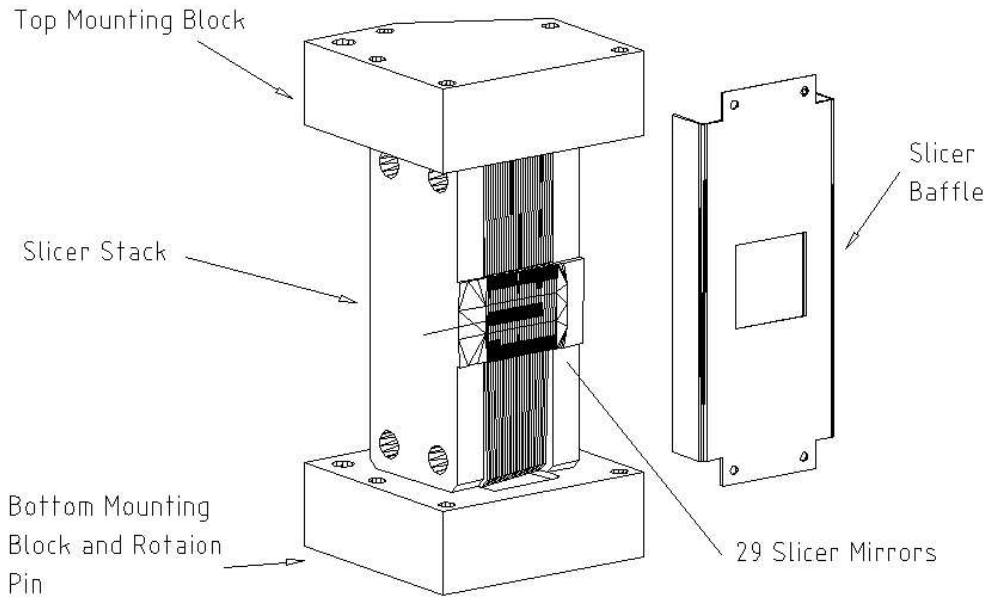

Figure 8: Imager slicer tower assembly with imager slicer baffle removed.

5.2 Mirror arrays

The mounting arrangement for the pupil and field mirror arrays is shown in Figure 9. The arrays will be machined and pinned to the mount such that they are pre-aligned. However, some adjustment is available in the support for each array

in case pre-alignment cannot be achieved. The mirror array blanks have a natural frequency in excess of 1000 Hz so cryocooler-induced oscillation should not be a problem.

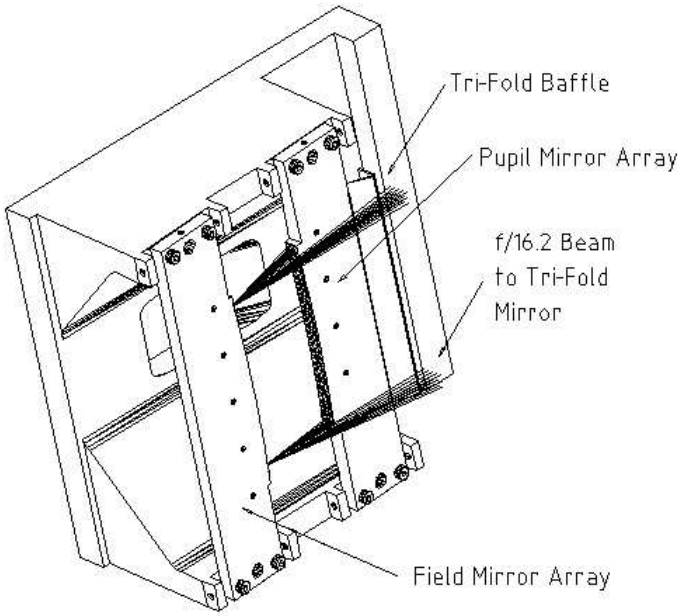

Figure 9: Pupil and field mirror arrays in their support structure.

6. CONCLUSIONS

The NIFS concentric IFU design delivers good image quality over a large number of IFU elements. The manufacture of monolithic mirror arrays by three-axis diamond machining solves many of the alignment issues inherent in multi-channel optical systems. The price that is paid for this simplification is the integration of the IFU with the spectrograph collimator in a dedicated IFU instrument, as well as relatively long optical path lengths. The latter is somewhat incompatible with a cryogenic instrument, but has been accommodated in NIFS.

REFERENCES

1. P. McGregor, J. Hart, P. Conroy, L. Pfitzner, G. Bloxham, D. Jones, M. Downing, M. Dawson, P. Young, M. Jarnyk, and J. van Harmelen, "Gemini near-infrared integral field spectrograph (NIFS)", *Proc. S.P.I.E.*, **4841**, 2002.
2. R. Content, "New design for integral field spectroscopy with 8-m telescopes", *Proc. S.P.I.E.*, **2871**, pp. 1295-1305, 1997.
3. R., Bacon, G. Adam, A. Baranne, G. Courtes, D. Dubet, J.P. Dubois, E. Emsellem, P. Ferruit, Y. Georgelin, G. Monet, E. Pecontal, A. Rousset, and F. Say, "3D spectrography at high spatial resolution. I. Concept and realization of the integral field spectrograph TIGER", *Astr. Ap. Suppl.*, **113**, pp. 347-357, 1995.
4. R. Bacon, Y. Copin, G. Monnet, B.W. Miller, J.R. Allington-Smith, M. Bureau, C.M. Carollo, R.L. Davies, E. Emsellem, H. Kuntschner, R.F. Peletier, E.K. Verolme, and P.T. de Zeeuw, "The SAURON project. I. The panoramic integral-field spectrograph", *M.N.R.A.S.*, **326**, pp. 23-35, 2001.
5. M.A. Kenworthy, I.R. Parry, and K. Taylor, "SPIRAL phase A: A prototype integral field spectrograph for the Anglo-Australian Telescope", *PASP*, **113**, pp. 215-226, 2001.
6. J. Allington-Smith, G. Murray, R. Content, G. Dodsworth, R. Davies, B.W. Miller, J. Turner, I. Jorgenson, I. Hook, D. Crampton, and R. Murowinski, "The GMOS integral field unit: First integral field spectroscopy with an 8 m telescope", astro-ph/0202330, 2002.
7. L. Weitzel, A. Krabbe, H. Kroker, N. Thatte, L.E. Tacconi-Garman, M. Cameron, and R. Genzel, "3D: The next generation near-infrared imaging spectrometer", *Astr. & Ap. Suppl.*, **119**, pp. 531-546, 1996.

8. F. Eisenhauer, M. Tecza, S. Mengel, N.A. Thatte, C. Röhrle, K. Bickert, and J. Schreiber, "Imaging the universe in 3D with the VLT: the next generation field spectrometer SPIFFI", *Proc. S.P.I.E.*, **4008**, pp. 289-297, 2000.